

MOLECULAR DYNAMICS SIMULATION
USING THE MODIFIED EMBEDDED
ATOM METHOD

By

KALYAN K. MAVULETI

Bachelor of Technology

Jawaharlal Nehru Technological University


Kakinada, India

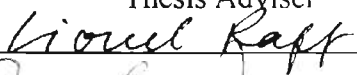
1998


Submitted to the Faculty of the
Graduate College of the
Oklahoma State University
in partial fulfillment
the requirements for
the Degree of
Master of Science
December, 2000

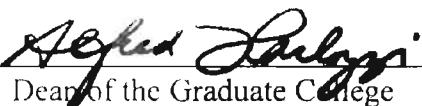
MOLECULAR DYNAMICS SIMULATION
USING THE MODIFIED EMBEDDED
ATOM METHOD

Thesis Approved:



Thesis Adviser






Dean of the Graduate College

ACKNOWLEDGEMENTS

First and foremost, I would like to thank my parents for their love, inspiration and emotional support at every stage of my life to help me grow and attain higher education. Special thanks are due to my fiancée whose love has provided me with the strength, confidence and motivation.

I would like to express my sincere appreciation to my advisor, Dr. Ranga Komanduri, for his constructive guidance, motivation, inspiration and support throughout my coursework. I would also like to express my sincere appreciation to Dr. Raff, for his intelligent advice and help with Molecular Dynamics (MD) and also for the numerous discussions we had during the present study and without whose help this project wouldn't have succeeded. I would also like to thank Dr. Price for agreeing to serve on my committee and for his invaluable guidance and advice.

The Molecular Dynamics (MD) code using the Modified Embedded Atom Method (MEAM) was developed and tested with Mr. David Stokes, a graduate student working under the guidance of Dr. Komanduri. Uniaxial tension simulations were conducted on various metals using this code to verify the validity of the developed MEAM model for MD simulation, which is the subject of the current report. I extend my

gratitude for his valuable assistance and co-operation during this project. I would also like to thank Mr. Naga Chandrasekaran, for his advice, encouragement, and valuable suggestions. Finally, I would like to thank all my friends and colleagues for their support and encouragement.

TABLE OF CONTENTS

Chapter	Page
I. INTRODUCTION	1
1.1 Introduction	1
1.2 Molecular Dynamics Simulation	2
II. LITERATURE REVIEW	5
2.1 Introduction to Tensile Testing at Microlevel	5
2.2 Molecular Dynamics Simulation	7
2.3 Modified Embedded Atom Method	11
III. PROBLEM STATEMENT	14
IV. MOLECULAR DYNAMICS SIMULATON	16
4.1 Molecular Dynamics Modeling	16
4.2 Numerical Integration	18
4.3 Choice of the Model	20
V. POTENTIAL MODEL	22
5.1 Modified Embedded Atom Method	22
5.2 Determination of Parameters	23
5.3 Determination of Forces	26
VI. VALIDATION OF THE POTENTIAL MODEL	27
6.1 Numerical vs. Analytical Forces	27
6.2 Conservation of Energy	28
6.3 Back Integration	33
VII. RESULTS AND DISCUSSION	35
7.1 Introduction	35
7.2 Tension Tests	35
7.3 Shear Test of Nickel	39
VIII. CONCLUSIONS	48
8.1 Testing for the Accuracy of the Software	48
8.2 Uniaxial Tension	49
8.3 Shear Test of Nickel	49
8.4 Future Work	50
REFERENCES	52

LIST OF TABLES

Table		Page
6.1	Comparison of analytical and numerical forces on atom 1 in x-direction	29
6.2	Comparison of analytical and numerical forces on atom 1 in y-direction	30
6.3	Comparison of analytical and numerical forces on atom 1 in z-direction	31
6.4	Conservation of energy test	32
7.1	Experimental conditions	35
7.2	Comparison of ultimate tensile strength values obtained by using the MEAM potential with those obtained by Komanduri et al (2000) and those quoted by Hertzberg (1996)	38

LIST OF FIGURES

Figure		Page
4.1	Illustration of Runge-Kutta method in action	21
6.1	Conservation of energy test	32
6.2	Path traced by atom 1 during forward and backward integration	34
6.3	Potential, kinetic and total energies during forward and backward integration	34
7.1(a)-(d)	Snapshots of the animation during tension test of nickel using the MEAM potential	41
7.2(a)-(d)	Snapshots of the animation during tension test of nickel using the Morse potential	42
7.3	Tension test of nickel using the Morse potential and MEAM potential	43
7.4	Stress vs. strain curves of nickel, copper, and iron using the MEAM potential	43
7.5(a)-(d)	Snapshots of the animation during tension test of copper using the MEAM potential	44
7.6(a)-(d)	Snapshots of the animation during tension test of iron using the MEAM potential	45
7.7 (a)-(d)	Snapshots of nickel in shear	46

7.8	Comparison of the shear stress/elastic shear modulus vs. shear Strain for nickel using the MEAM potential with that obtained by Horstemeyer (1999)	47
-----	--	----

NOMENCLATURE

A_i	scaling factor for embedding energy
E_i^0	sublimation energy (eV)
E_{tot}	total energy of the system (eV)
$F_{x_{ij}}$	x -component of the force on atom i due to atom j
$F_{y_{ij}}$	y -component of the force on atom i due to atom j
$F_{z_{ij}}$	z -component of the force on atom i due to atom j
N	total number of atoms
R	distance between the atoms (\AA^0)
R_i^0	equilibrium nearest neighbor distance (\AA^0)
R_{ij}	distance between atoms i and j (\AA^0)
R_{ij}^α	α component of the distance vector between atoms i and j .
V_{tot}	total potential energy of the system (eV)
Z_i	number of nearest neighbors
m_i	mass of atom i (atomic mass unit)
p_i	momentum of atom i
\dot{p}_i	force on atom i (eV/ \AA^0)
q_i	Cartesian coordinates of atom i
\dot{q}_i	velocity of atom i (\AA^0 /time unit)

- $s_i^{(l),0}$ geometry factors
- $t_i^{(l)}$ weighting factors for the atomic densities
- x_0 initial position of the atom
- x_i x-coordinate of atom i
- x_{ij} x-component of the distance between the atoms i and j
- x_{ij}^α ratio of α component of the distance vector between atoms i and j and the distance between atoms i and j .
- y_i y-coordinate of atom i
- y_{ij} y-component of the distance between the atoms i and j
- z_i z-coordinate of atom i
- z_{ij} z-component of the distance between the atoms i and j
- α_i exponential decay factor for the universal energy function
- $\beta_j^{(l)}$ exponential decay factors for the atomic densities
- ρ_i background electron density of atom i
- $\bar{\rho}_i$ total background electron density
- $\rho_i^{(l)}$ partial background electron density of atom i

Chapter 1

INTRODUCTION

1.1 INTRODUCTION

The industry of micromachining is in its infancy today, just as the Very Large Scale Integrated (VLSI) industry has been developing quickly since the late 70's. As design tools made the development of the Integrated Circuit (IC) industry possible, design tools will make the development of new components possible, which will combine the physical world needs of sensing and actuators with the rapidly growing capabilities of information technology. Microelectromechanical systems (MEMS) are miniature electromechanical sensor and actuator systems developed from the mature batch-fabricated processes of VLSI technologies. MEMS have wide applications such as miniature inertial measurement units, biochemical analysis on a chip, arrayed micromanipulation of parts, optical displays and micro-probes for neural recording. The current and increasing success of MEMS stems from their promise of better performance, low manufacturing costs, miniaturization and their capacity for integration with electronic circuits. The MEMS market is conservatively projected to reach between \$12 and \$14 billion by the end of this year. Micro-optics and MEMS are paving the way for

Micro-Opto-Electro-Mechanical Systems (MOEMS). Using MOEMS technology, micro-optical elements are batch-fabricated on chips concurrently with microsensors and microactuators to form integrated microsystems. MOEMS technology is highly attractive for commercial applications, since it leverages the integrated circuit infrastructure, which enables high volume production of microsystem components at a low manufacturing cost.

Uniaxial tension is the most direct way of evaluating mechanical properties of materials such as the elastic properties, the character and extent of plastic deformation, yield and tensile strengths, and toughness. Tensile tests are most common in determining the mechanical properties at macro level. However, when it is applied to thin film materials used in MEMS devices, many problems arise:

1. Alignment of the specimen in the testing machine is not easy to perform.
2. Gluing the specimen to the machine is not reliable.
3. Manipulation of the thin film specimen may cause irreparable mechanical damage.
4. It is very costly to perform nano-regime tensile testing due to complexity of the equipment.
5. Production of defect free materials in the form of tensile specimens is very difficult.

Thus it is very difficult to perform tensile testing of these devices. An alternative approach would be Molecular Dynamics Simulation, which is very easy to perform and is inexpensive.

1.2 MOLECULAR DYNAMICS SIMULATION

The essence of Molecular Dynamics (MD) is simply stated: numerically solve the N-body problem of classical mechanics. Molecular Dynamics started way back in the 1950's, but widespread attention was given only in the late 1970's. Even then it was possible only in some of the big national labs which had super-computers. But today with the advent of low cost powerful workstations with fast processors (e.g. the Digital Alpha workstation with 500 MHz clock speed used in this project) and parallel computing, it is possible to construct large scale MD simulations.

Molecular Dynamics Simulation brings together ideas from several disciplines. Knowledge of classical mechanics, vector analysis, numerical analysis, thermodynamics, and programming is essential. Also, a good understanding of the manufacturing processes is required to analyse the results. MD simulation is basically calculating the trajectories of the atoms by solving the differential equations of motion. MD predicts the motion of a given number of atoms governed by their mutual interatomic interactions described by a continuous potential function and requires the numerical integration of Hamilton's Classical equation of motion. A potential model is required to determine the forces on each atom due to its neighbours. Until recently, the Morse Potential was used to represent the potential between two atoms. It is a pair potential and represents FCC materials fairly well, but when it comes to BCC materials it does not represent the deformation behaviour well(Komanduri et al (2000)). So, a better potential model is required to represent all the materials. The Modified Embedded Atom Method (MEAM) developed by Baskes (1992)

represents the material properties better than the Morse Potential and is applicable to almost the whole range of metals. Pair potentials like the Morse Potential yield the total energy directly, but need the volume dependant energy to describe the elastic properties of a metal. If the volume is not represented properly, it may invalidate the results of a pair-potential calculation because the elastic properties of the solid are not represented accurately. In the Modified Embedded Atom Method, every atom is considered as an impurity, embedded in a host lattice consisting of all other atoms. This allows calculations using electron densities and allows realistic treatment of impurities in structures that include cracks, surfaces, and alloying additions.

Chapter 2

LITERATURE REVIEW

2.1 INTRODUCTION TO TENSILE TESTING AT MICROLEVEL

With the advent of thin film materials like silicon wafers used in the semiconductor industry, it is becoming increasingly necessary to perform tensile testing at micro level to determine how the materials would react under load. Sato et al. (1998) performed uniaxial tensile testing of a single-crystal silicon film on a silicon chip. They proposed a *tensile testing procedure*, in which the external load is applied perpendicular to the loading lever, by which the film specimen is uniaxially stretched in the horizontal direction which is given in figures 2.1 and 2.2. This method allowed the tensile testing of single crystal silicon film having any arbitrary orientation. They showed that the load linearly increased until the specimen fractured. When the fracture occurred, the load dropped to equal that of the rotational stiffness of the torsion bars. They performed uniaxial tensile testing on three differently oriented specimens and measured Young's modulus and fracture strain for each orientation. The measured values were in close agreement with the calculated values of bulk materials.

The direct tension tests, like the one described above, are effective only when properly performed. The set up requirements for testing, such as alignment and deflection

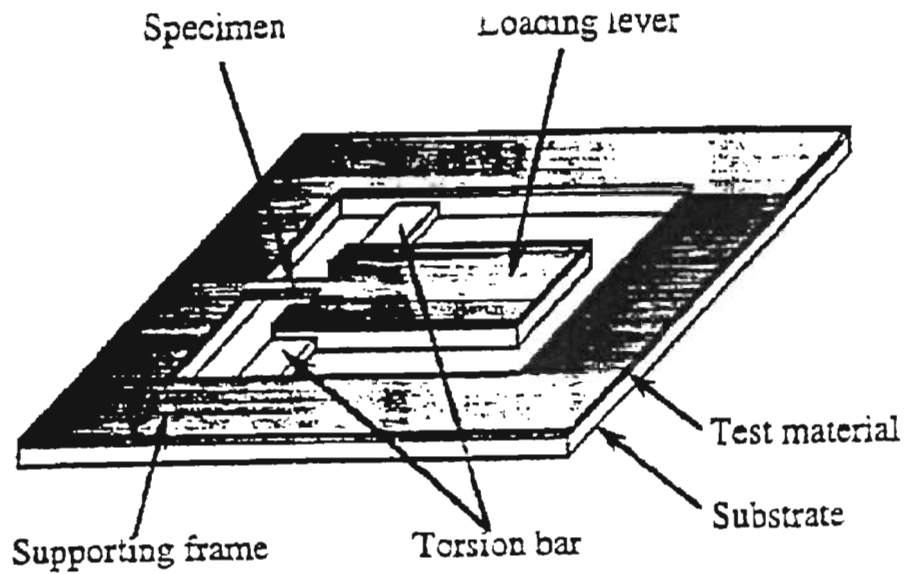


Figure 2.1 The on-chip tensile testing method: chip structure [Sato et al. (1998)]

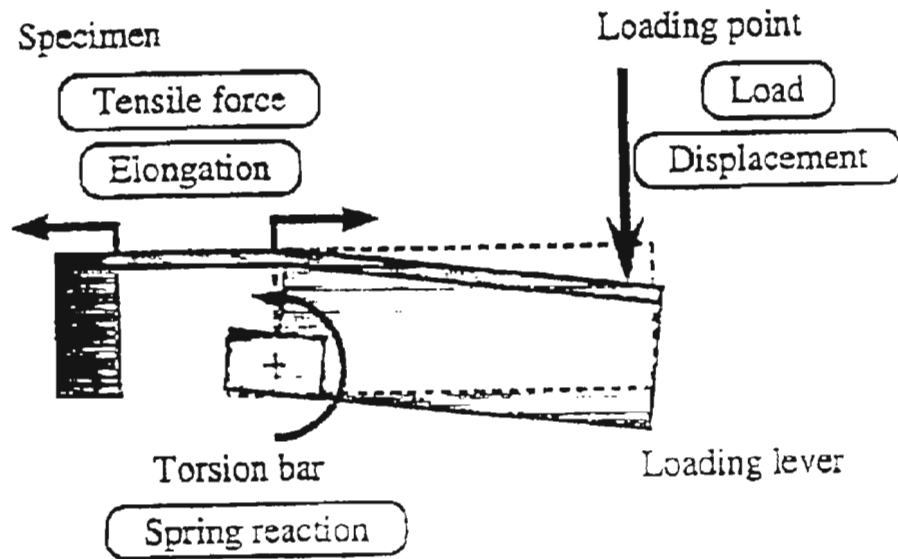


Figure 2.2 The on-chip tensile testing method: cross section of the chip [Sato et al. (1998)]

measurement, are difficult to meet for micro-scale test samples. Yi et al. (2000) proposed a new method in which a load cell measured the induced force and the strain was measured by a laser interferometry system. The advantage of the optical method was that

the strain was obtained without physical contact to the sample. The specimen was etched by four different common silicon etchants - KOH, EDP, TMAH and XeF₂. The Young's modulus measured, 169.2 ± 3.5 GPa, was very close to the widely accepted value of 168.9 GPa for silicon.

2.2 MOLECULAR DYNAMICS SIMULATION

Eyring and his colleagues (1944) performed the first trajectory calculations of H and H₂ molecules. All the calculations were performed manually since there were no computers available during that time. They found that the system was caught in a local minimum and oscillated in that minimum without escaping out. Later, Alder and Wainwright (1959) devised molecular dynamics in the late 1950's, which is one of the forms of equilibrium molecular dynamics. It is typically applied to an isolated system containing a fixed number of molecules N in a fixed volume V . Because the system is isolated, the total energy E (sum of Potential and Kinetic energies) is also constant. The first applications of MD techniques for molecular simulation were made for simple fluids. Another form of molecular dynamics, non-equilibrium molecular dynamics, first appeared in the early 1970's. In these methods, an external force is applied to the system to establish the non-equilibrium situation of interest, and the system's response to the force is determined from the simulation. MD simulation has been applied to various fields like crystal growth, reactive scattering and simulation of complex liquids in chemistry, simulations for energetic and structural features of biological systems, and in

machining for tension, indentation, cutting and friction at the atomic scale. The available literature is vast, only the literature concerning the tension and shear is reviewed.

Lynden-Bell (1994, 1995) investigated the behavior of FCC crystals of the metals platinum, gold, rhodium and silver under uniaxial tension using the Finnis-Sinclair potential. The study was conducted for the variation of potential energy and longitudinal stress with strain for the above materials at four different temperatures $0.04T_m$, $0.35 T_m$, $0.55 T_m$, $0.7 T_m$, where T_m was the bulk melting temperature of the material. Void formation and growth of nano-cracks were reported which were the causes of failure. The stress was reported to increase to a maximum at low temperatures and then decreased due to a series of structural rearrangements. Platinum and gold, which were highly ductile, were reported to develop local regions of disorder first when compared to the not-so-ductile rhodium and silver. However, at temperatures above half the melting point, all the metals were reported to be disordered before failure, by void formation. For the investigation at different temperatures, it appeared that both the short and long range terms for interactions were needed. So, a potential model with many-body terms would have better represented the behavior of the material in bulk.

Rentsch and Inaski (1995) conducted MD simulation of silicon under uniaxial tension using the Tersoff potential. They reported a linear stress-strain relationship followed by a sudden break down to zero. Anisotropic deformation of silicon was reported. The Young's modulus was found to be 171 GPa and the specific surface energy to be 0.393 Jm^{-2} .

Kitamura et al (1997) performed MD simulation of nano-single crystal of nickel in tension using the embedded atom potential. Tension tests were carried out under two conditions: (1) tension without constraint of transverse deformation and (2) tension with constraint of transverse deformation. In the first case, yielding was brought about by the crystallographic slip on the $\{111\}$ planes at a strain of 0.1. The yield stress in tension was about 15 – 20 GPa and very little differences were noticed among the wire, film and bulk samples. The multiple slip on the $\{111\}$ planes continued to take place after the yield. The plastic deformation caused ductile shear fracture. With constraints, the yield stress reached 40 GPa. No plastic strain was generated. A cleavage crack initiated and brought about brittle fracture. It was reported that the constraint changed the fracture mode.

Heino et al (1998) studied the mechanical properties of copper by MD using the effective medium theory as the potential model. Simulations of point defects, grain boundary, and a larger void, which served as the seed for crack propagation, were studied at room temperature. A decrease in fracture stress and strain, and tensile modulus was reported with an increasing number of defects. Systems with larger number of defects were reported to appear more isotropic than ordered systems, in terms of tensile modulus. They reported that the systems with grain boundaries were weaker than the ordered systems in terms of modulus, fracture stress and fracture strain. With thick systems, with free boundaries and an initial large void, the $\{111\}$ slip plane was reported to propagate in a $\langle 110 \rangle$ direction with a speed of about 60% of the longitudinal speed of the sound for the specific crystal orientation. With thin systems, including a crack seed and having free

boundaries, crack propagation was reported in the $\langle 110 \rangle$ direction by microvoid coalescence.

Komanduri et al (2000) studied the uniaxial tension of single-crystal materials, both FCC [Al, Cu, and Ni] and BCC [Fe, Cr, and W] using the Morse Potential. They reported a rapid increase in stress up to a maximum followed by a gradual drop to zero when the specimen failed by ductile fracture. They also reported that the radius of the neck increased with an increase in the deformation of the specimen and decreased as the ductility of the material decreased. Rapid fluctuations in the force values were reported. The strain to fracture was reported to be lower for BCC materials than FCC materials. Tungsten had the highest strength and aluminum had the lowest strength. The ultimate tensile strength of Cu, Ni, Al, Fe, Cr, and W were reported to be ~28, 36, 13, 29, 31, and 51 GPa, respectively. The strain to fracture was reported to be ~2.17, 1.67, 3.2, 1.52, 1.52, and 1.4 for Cu, Ni, Al, Fe, Cr, and W, respectively. They also reported a good correlation between the D - and α - parameters of the Morse potential with the ultimate tensile strength and the strain to fracture for the FCC materials, and no such correlation for the BCC materials. They suggested that an alternate potential model should be used for BCC materials since the deformation behavior wasn't represented well by the Morse potential.

Horstemeyer and Baskes (1999) performed atomistic finite deformation using the Embedded Atom Method. They observed a spatial size scale effect on the yield stress. They observed that the mechanical yield point occurred from dislocation initiation at the

edge of the numerical specimens. They also observed that, as the spatial length scale increased, the continuum rotational effect coupled with the increase in the dislocation population reduced the oscillatory behavior. They proposed a length scale bridging idea by relating a continuum single degree of freedom loss coefficient, which related the plastic energy to the total strain energy, to varying sizes of blocks of atoms.

By the above review, it is clear that a potential model which is good for all the metals, FCC, BCC, diamond structure and HCP, must be used for MD simulation. Modified Embedded Atom Method (MEAM) is one such potential model and is considered in this project.

2.3 MODIFIED EMBEDDED ATOM METHOD

The first step towards the present day MEAM was the quasiautom theory proposed by Stott and Zaremba (1982), that was used successfully to calculate the characteristics of hydrogen in metals. They proposed that "the energy of an impurity in a host is a function of the electron density of the unperturbed (i.e. without impurity) host".

Daw and Baskes (1984) generalized the quasiautom theory to treat all atoms in a unified way, and called it the embedded atom method. They proposed that, every atom is considered as an impurity, embedded in a host lattice consisting of all other atoms. This allowed calculations using electron densities and allowed realistic treatment of impurities in structures that include cracks, surfaces, and alloying additions. The electron densities

were approximated by the linear superposition of spherically averaged atomic electron densities. They also proposed that the embedding energy of the atom depends only on the environment immediately around the impurity, i.e. impurity experiences a locally uniform electron density. The energy was given by

$$E_{tot} = \sum_i F_i(\rho_i(R_i)) + \frac{1}{2} \sum_{i,j} \phi(R_{ij}) \quad (1)$$

Where ρ_i was the electron density of the host atom without atom i , and ϕ was the short-range electrostatic pair potential. From this expression for the total energy of a given metal, several ground state properties like lattice constant, elastic constants, sublimation energy, and vacancy-formation energy were calculated. The validity of the above functions was tested by computing a wide range of properties, like the formation volume and migration energies of vacancies, the formation energy, the migration energy of divacancies and self-interstitials, the surface energy and geometries of the low-index surfaces of the pure metals, and the segregation energy of substantial impurities to $\{100\}$ surfaces. The embedded atom method developed by Daw and Baskes was based on the density functional theory and the electron density was approximated as a linear superposition of electron densities. These assumptions are better approximations for FCC metals but not for BCC metals.

Adams and Foiles (1990) extended the embedded atom method to BCC material Vanadium. Since the electron density in BCC metals was not well approximated by linear superposition of electron densities, the authors used the adjustable electron density proposed by Voter and Chen (1987). This theory was adopted since spherically

symmetric electron densities were easier to incorporate in the model. The pair term in Eq (1) was assumed to have the form of the Morse Potential.

Later on, Baskes (1987) modified the embedded atom method to include directional bonding and applied it to silicon. Baskes, Nelson and Wright (1989) extended the silicon embedded atom method to the silicon-germanium system. This extended method was called modified embedded atom method. This method had a few deficiencies when it was initially developed. There was inward relaxation at a vacancy, an extremely large stacking fault energy and only qualitatively accurate small cluster predictions. These deficiencies were partially resolved in the later paper by Baskes (1992). The common attribute of all the papers is that the interaction between two atoms depends on the local environment.

The MEAM has been applied to metals and semiconductors and also for diatomic gaseous elements. In this method, simplification to the first nearest neighbors is possible, which reduces the computational time. The difference between the EAM and MEAM is that the ρ_i , which is given as the linearly superposition of spherically averaged atomic electron densities in EAM is augmented by an angularly dependent term in MEAM. Baskes and Nelson (1994) have extended MEAM to HCP materials. So, MEAM is much more versatile and can be used for FCC, BCC, diamond structures, and HCP metals.

Chapter 3

PROBLEM STATEMENT

MD simulation has been used to conduct uniaxial tension of different materials using different potential models like the Finnis-Sinclair potential (Lynden-Bell [1994,1995]), the Tersoff potential (Rentsch and Inasaki [1995]), the Morse potential (Komanduri et al. [2000]), and the effective medium theory (Heino et al. [1998]). Using the Finnis-Sinclair potential, it appeared that a potential model with many body terms would have better represented the behavior of the material in bulk. When the Morse potential was used for MD simulations, good correlation was found between the D - and α - parameters of the Morse potential with the ultimate tensile strength and strain to fracture for the FCC materials. No such correlation was found for BCC materials. So, a potential model which can represent the bulk properties of metals fairly accurately, and which can be used for the whole range of metals should be used for MD simulations. The embedded atom method and the MEAM are such potential models. The difference between these models is that the linear superposition of atomic electron densities in the embedded atom method is augmented by an angularly dependent term in the MEAM. Thus MEAM potential is chosen as the potential model for MD simulation. The objective of this study is to:

1. Develop the software for MD using the MEAM as the potential model for the trajectory calculations
2. To find the forces on the atoms by calculating the derivatives of the total potential with respect to the three coordinate axes, x, y and z.
3. To validate the software by different testing procedures like the numerical vs. the analytical force test, the conservation of energy test and the back integration test, to validate the accuracy of the model.
4. To perform a shear test of Nickel to evaluate the shear stress and strain and to observe the deformation during the simulation.
5. To perform uniaxial tension calculations using MD for various FCC and BCC metals and to find the ultimate tensile strength and the strain to fracture of these metals and, also, to observe the deformation and necking during the simulation.

Chapter 4

MOLECULAR DYNAMICS SIMULATION

Molecular dynamics simulation basically involves the calculation of trajectories. This calculation involves the numerical integration of classical equations of motion for a system of interacting atoms over a period of time. The time step used in this integration is of the order of 10^{-15} sec, which is less than the period of vibration of the atoms.

4.1 MOLECULAR DYNAMICS MODELING

Consider an isolated system comprising N bodies with the coordinates (x_i, y_i, z_i) where $i = 1, 2, 3, \dots, N$. Given a set of N independent generalized coordinates and velocities $\{q_i, \dot{q}_i\}$ that describe the state of a conservative system (one in which all the forces derive from some potential energy function U), so that $L = L(\{q_i\}, \{\dot{q}_i\}, t)$, then L can be shown to satisfy the Lagrange equations

$$\frac{d}{dt} \left(\frac{\partial L}{\partial \dot{q}_i} \right) - \frac{\partial L}{\partial q_i} = 0, i = 1, \dots, N \quad (4.1)$$

These equations are the starting point for many of the subsequent developments. Newton's second law is a simple consequence of this result. where, if q_i denotes a

component of the Cartesian coordinates for one of the atoms (and assuming identical masses m):

$$L = \frac{1}{2} m \sum_i \dot{q}_i^2 - V(\{q_i\}) \quad (4.2)$$

So that equation (4.1) becomes

$$m\ddot{q}_i = -\partial V/\partial q_i = F_i \quad (4.3)$$

Where F_i is the corresponding force component.

By replacing the generalized velocities $\{\dot{q}$ in the Lagrange formulation by the generalized momenta $p_i = \partial L/\partial \dot{q}_i$ (if the coordinates are Cartesian, then $p_i = m\dot{q}_i$) and consider the Hamiltonian $H = H(\{q_i\}, \{p_i\}, t)$ defined by

$$H = \sum_i \dot{q}_i p_i - L \quad (4.4)$$

The two first order equations of motion associated with each coordinate are

$$\dot{q}_i = \frac{\partial H}{\partial p_i} \quad (4.5)$$

$$\dot{p}_i = -\frac{\partial H}{\partial q_i} \quad (4.6)$$

If H has no explicit time dependence, then $\dot{H} = 0$, and H - the total energy - is a conserved quantity.

From the above equations (4.5) and (4.6), we get the following differential equations for each atom in the three coordinate systems.

$$\partial H / \partial P x_i = dx_i / dt = p x_i / m_i \quad (4.7)$$

$$\partial H / \partial P y_i = dy_i / dt = p y_i / m_i \quad (4.8)$$

$$\partial H / \partial P z_i = dz_i / dt = p z_i / m_i \quad (4.9)$$

$$\partial H / \partial x_i = \partial V / \partial x_i = dp x_i / dt \quad (4.10)$$

$$\partial H / \partial y_i = \partial V / \partial y_i = dp y_i / dt \quad (4.11)$$

$$\partial H / \partial z_i = \partial V / \partial z_i = dp z_i / dt \quad (4.12)$$

So the total number of differential equations to be solved are $6N$. The following are the system of units used in the above equations

$$1 \text{ mass unit} = 1 \text{ atomic mass unit} = 1.007/6.023 \times 10^{23}$$

$$1 \text{ distance unit} = 1 \text{ \AA} = 10^{-8} \text{ cm}$$

$$1 \text{ energy unit} = 1 \text{ eV} = 23.06 \text{ kcal/mol} = 4.184 \times 23.06 \text{ kJ/mol}$$

$$1 \text{ time unit} = 1 \text{ t.u.} = 1.018 \times 10^{-14} \text{ sec.}$$

4.2 NUMERICAL INTEGRATION

The calculation of trajectories requires the numerical integration of the equations (4.7) through (4.12) from an initial state in the configuration space identified as reactants to some final state associated with products. The various numerical techniques used are:

1. Fourth order Runge-Kutta method (which is self starting)
2. Fifth, sixth etc order predictor-corrector methods (non self starting)
3. Variable step size methods.

Runge-Kutta method has several advantages when compared to the other methods.

1. It is self-starting, so it is unnecessary to know the values of elements prior to $t = t_0$.
2. The integration error is very small, of the fourth order, $O(h^4)$. So the error can be neglected without affecting the results significantly.
3. The method is stable and fairly easy to program.

Its main disadvantage is:

1. The need to compute a large number of derivatives ($24N$) for each integration step, which demands a lot of computer time

Though this is a disadvantage, it is worth it because of the greater accuracy and the stability of the method. Other methods, like Predictor-Corrector methods, have the advantage of providing an automatic error estimate at each integration step, thus allowing the program to use variable step size to achieve the specified accuracy. However, these methods are not self-starting and require the use of Runge-Kutta method to start the integration. So, the Runge-Kutta method was chosen for the calculations.

If there are N particles whose initial derivatives $D1 = f(x_0, y_0)$ are known and we integrate them over a period of time t , the Runge-Kutta method involves the calculation by the following steps.

1. Move them to a new position $P2$ using $D1$ and a time step of $t/2$, so that

$$D2 = f(x_0 + \Delta x/2, y_0 + D1 * \Delta x/2)$$
2. Get them back to their original positions and move them to their new positions $P3$ using the derivatives $D2$ and calculate $D3 = f(x_0 + \Delta x/2, y_0 + D2 * \Delta x/2)$
3. Get them back to their original positions and move them to their new positions based on derivatives $D3$ and a time step of t and calculate $D4 = f(x_0 + \Delta x/2, y_0 + D3 * \Delta x/2)$

4. Compute the average derivative $\langle D \rangle = [D1 + D2*2 + D3*2 + D4]/6.0$ and then compute the $\Delta y = \langle D \rangle * \Delta x$ and $y1 = y_0 + \Delta y$, to get them to their final positions

Figure 4.1 illustrates this point. This is a simultaneous approach in the sense that all the particles are moved during the above steps. Thus, for a set of N particles, there will be $4N$ intermediately calculated positions and forces for a Runge-Kutta procedure time step.

The interatomic potential used in the simulation to model the materials plays an important role in determining the accuracy of simulation results. The modified embedded atom method is used in the present calculations, which is explained in the next chapter.

4.3 CHOICE OF THE MODEL

The following are some of the important considerations in the choice of the model for MD simulations:

1. The number of differential equations to be evaluated for a system of N atoms, which is $6N$. So, if there are 1000 atoms, we need to integrate 6000 first order coupled differential equations. This provides a restriction on the computer memory and computational time. So, we need to choose a model within these restrictions
2. Number of terms in the potential energy hypersurface that are to be considered. For example, in a pair potential it is $N(N-1)/2$ and for a many body potential like the Modified embedded atom method, it is $N(N-1)$
3. Size convergence should be considered so that the results are independent of our choice of N .

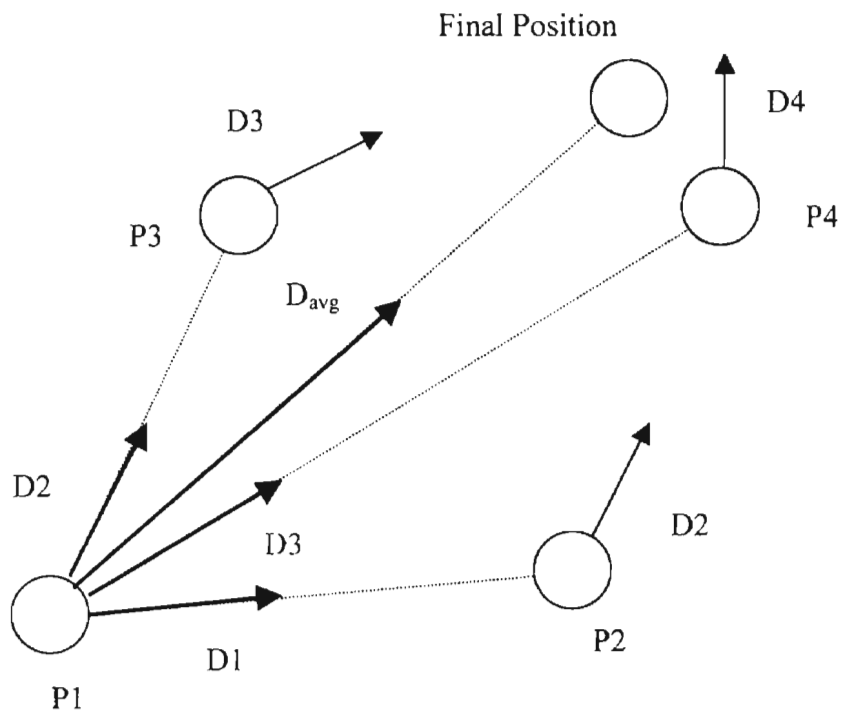


Figure 4.1 Illustration of Runge-Kutta Method in action

Chapter 5

POTENTIAL MODEL

The choice of the potential model to be used in the trajectory calculation is very important since it has to represent the properties of materials in bulk. The modified embedded atom method is a good choice in the sense that it represents the properties of bulk materials better than other pair potentials, like Morse or Lennard Jones potentials.

5.1 MODIFIED EMBEDDED ATOM METHOD

The total energy E of a system of atoms given by the embedded atom method is:

$$E_{tot} = \sum_i F_i(\rho_i(R_i)) + \frac{1}{2} \sum_{i,j} \phi(R_{ij}) \quad (5.1)$$

The first term in the right side of the equation is the embedding function, i.e., the energy to embed an atom of type i into the background electron density at site i , $\bar{\rho}_i$, and the second term is the pair interaction between the atoms i and j , whose separation is given by R_{ij} . According to the embedded atom method, $\bar{\rho}_i$ is the linear supposition of spherically averaged atomic electron densities. In the modified embedded method, it is augmented by an angularly dependent term. The energy for an individual atom is given

$$E_i = F_i(\rho_i / Z_i) + \frac{1}{2} \sum_j \phi_{ij}(R_{ij}) \quad (5.2)$$

The background electron density is renormalized by dividing it by the number of nearest neighbors Z_i .

The pair interaction is given by the equation

$$\phi_{ij}(R) = \frac{2}{Z_i} \{E_i^u(R) - F_i(\bar{\rho}_i^0(R) / Z_i)\} \quad (5.3)$$

From the above three equations the energy of an atom E_i is given by

$$E_i = \frac{1}{Z_i} \sum_{j(\neq i)} E_i^u(R_{ij}) + \left[F_i(\bar{\rho}_i / Z_i) - \frac{1}{Z_i} \sum_{j(\neq i)} F_i(\bar{\rho}_i^0(R_{ij}) / Z_i) \right] \quad (5.4)$$

The first part of the above equation is the average of the energy per atom, of the reference lattice at each of the nearest-neighbor distances. The second part is the difference between the embedding energy at the background electron density actually seen by the atom i and the average embedding energy of this atom in the reference lattice, at each of the nearest-neighbor distances.

5.2 DETERMINATION OF PARAMETERS

The equation (5.3) has three terms and each of the terms can be determined in the following way. In the first term Z_i is the number of nearest neighbors and E_i^u is given by

$$E_i^u(R) = -E_i^0 (1 + a^*) e^{-a^*} \quad (5.5)$$

$$a^* = \alpha_i (R / R_i^0 - 1) \quad (5.6)$$

Where

α_i = exponential decay factor for the universal energy function ?

E_i^0 = sublimation energy (eV)

R = distance between the atoms (\AA)

R_i^0 = equilibrium nearest neighbor distance (\AA)

In the second term, the function F is given by

$$F_i(\rho) = A_i E_i^0 \rho \ln \rho \quad (5.7)$$

So the second part becomes

$$F_i(\bar{\rho}_i / Z_i) = A_i E_i^0 (\bar{\rho}_i / Z_i) \ln(\bar{\rho}_i / Z_i) \quad (5.8)$$

Where

$\bar{\rho}_i$ = total background electron density

A_i = scaling factor for embedding energy

E_i^0 = sublimation energy (eV)

The total background electron density is given by

$$(\bar{\rho}_i)^2 = \sum_{l=0}^3 t_i^{(l)} (\rho_i^{(l)})^2 \quad (5.9)$$

Where

$t_i^{(l)}$ = weighting factors for the atomic densities

The first partial background electron density at site i is given by

$$\rho_i^{(0)} = \sum_{j(\neq i)} \rho_j^{a(0)}(R_{ij}) \quad (5.10)$$

Where the atomic electron density of type- j atom at a distance R_{ij} from site i is given by

$$\rho_j^{a(l)}(R_{ij}) = e^{-h^*} \quad (5.11)$$

$$e^{-h^*} = \beta_j^{(l)} (R_{ij} / R_i^0 - 1) \quad (5.12)$$

$\beta_j^{(l)}$ = exponential decay factors for the atomic densities

R_i^0 = equilibrium nearest distance (\AA)

R_{ij} = distance between atoms i and j (\AA)

Similarly the second, third and fourth partial electron densities are given by

$$(\rho_i^{(1)})^2 = \sum_{\alpha} \left[\sum_{j(\neq i)} x_{ij}^{\alpha} \rho_j^{a(1)}(R_{ij}) \right]^2 \quad (5.13)$$

$$(\rho_i^{(2)})^2 = \sum_{\alpha, \beta} \left[\sum_{j(\neq i)} x_{ij}^{\alpha} x_{ij}^{\beta} \rho_a^{(2)}(R_{ij}) \right]^2 - \frac{1}{3} \left[\sum_{j(\neq i)} \rho_j^{a(2)}(R_{ij}) \right]^2 \quad (5.14)$$

$$(\rho_i^{(3)})^2 = \sum_{\alpha, \beta, \gamma} \left[\sum_{j(\neq i)} x_{ij}^{\alpha} x_{ij}^{\beta} x_{ij}^{\gamma} \rho_j^{a(3)}(R_{ij}) \right]^2 \quad (5.15)$$

Where $x_{ij}^{\alpha} = R_{ij}^{\alpha} / R_{ij}$, and R_{ij}^{α} is the α component of the distance vector between atoms i and j . The above equations are chosen so that the partial background electron densities are invariant to lattice translation and rotation, scale simply with atomic electron density for homogeneous deformation, and equal zero for a cubic lattice.

In the third term, the function F is given by

$$F_i(\bar{\rho}_i^0(R_{ij})/Z_i) = A_i E_i^0(\bar{\rho}_i^0(R_{ij})/Z_i) \ln(\bar{\rho}_i^0(R_{ij})/Z_i) \quad (5.16)$$

Where

$$(\bar{\rho}_i^0(R_{ij}))^2 = \sum_{l=0}^3 t_i^{(l)} s_i^{(l),0} (\rho_i^{a(l)}(R_{ij}))^2 \quad (5.17)$$

$s_i^{(l),0}$ = geometry factors

The rest of the terms are the same as explained above.

All the prior terms are put together to obtain the final equation, i.e., the total potential of the system. The next step is to determine the forces between the atoms from the potential function.

5.3 DETERMINATION OF FORCES

The determination of forces is crucial and time consuming because of the complexity of the potential function. The force on an atom i due to atom j is obtained by differentiating the total potential with respect to x, y, and z-components of the distance between the atoms i and j , to get the force in x, y and z directions respectively.

Force in x-direction,

$$F_{x_{ij}} = -\frac{\partial V_{tot}}{\partial x_{ij}} \quad (5.18)$$

Similarly, in y and z-directions

$$F_{y_{ij}} = -\frac{\partial V_{tot}}{\partial y_{ij}} \quad (5.19)$$

$$F_{z_{ij}} = -\frac{\partial V_{tot}}{\partial z_{ij}} \quad (5.20)$$

Once the potential and forces are obtained, the model is to be tested to validate the accuracy of the model.

Chapter 6

VALIDATION OF THE POTENTIAL MODEL

Once the software for the MD simulation is developed, i.e., the potential and the forces are determined; it has to be tested before it is used. There are many ways of testing the model for different parameters like numerical vs. analytical forces test for the validation of the forces, the conservation of energy test and the back integration test.

6.1 NUMERICAL vs. ANALYTICAL FORCES

The first and foremost thing is to validate the force function. This is done by comparing the analytical forces, got from the derivatives of the potential, to the numerical forces derived from the formula:

$$\left. \frac{dV}{dx} \right|_{x=x_n} = 0.75 \times S_1 - 0.15 \times S_2 + 0.01666666667 \times S_3 \quad (6.6)$$

$$S_1 = [V(x_0 + \Delta x) - (x_0 - \Delta x)] / \Delta x \quad (6.7)$$

$$S_2 = [V(x_0 + 2\Delta x) - (x_0 - 2\Delta x)] / \Delta x \quad (6.8)$$

$$S_3 = [V(x_0 + 3\Delta x) - (x_0 - 3\Delta x)] / \Delta x \quad (6.9)$$

The testing sample contains five atoms, which are placed in the following configuration (2.0, 2.0, 0.0), (2.0, -2.0, 0.0), (-2.0, 2.0, 0.0), (-2.0, -2.0, 0.0), (0.0, 0.0, 2.0). The atom 1 is moved to 1 \AA in steps of 0.1 \AA and the forces are calculated at each step. The numerical and analytical forces agree well, demonstrating that the analytical forces are right. The tables 6.1 through 6.3 show the comparison between analytical vs. numerical forces in x, y and z directions respectively

6.2 CONSERVATION OF ENERGY

After the validation of the force function, it is necessary to check if the system conserves energy. If there are no external forces acting on the system, and if the model is allowed to integrate for the given period of time, the sum of potential and kinetic energies which is the total energy must remain constant. This test is necessary, as it not only validates the accuracy of the potential and forces functions but also the integration procedure, i.e., the Runge-Kutta procedure.

For this test, the sample is one lattice of Nickel, which has 14 atoms. This sample is allowed to integrate for 10 time units and the values are given in the table 6.4. The total potential is constant for up to 12 significant digits. The same is shown in the figure 6.1

Table 6.1 Comparison of analytical and numerical forces on atom 1 in x-direction

Distance moved by atom 1 in the positive x direction	Analytical force on atom 1 in the x-direction	Numerical force on atom 1 in the x-direction	Analytical force on atom 2 in the x-direction	Numerical force on atom 2 in the x-direction
0	0.317994486191	0.317994486191	0.146299010461	0.146299010461
0.1	0.392243426220	0.392243426220	0.150204136858	0.150204136858
0.2	0.443425449382	0.443425449382	0.156172952299	0.156172952299
0.3	0.478482723558	0.478482723558	0.163469672011	0.163469672011
0.4	0.501392714854	0.501392714854	0.171538306544	0.171538306544
0.5	0.514487845642	0.514487845642	0.179955816315	0.179955816315
0.6	0.519309615179	0.519309615179	0.188397761492	0.188397761492
0.7	0.517073341564	0.517073341564	0.196614201357	0.196614201357
0.8	0.508875262056	0.508875262056	0.204413074192	0.204413074192
0.9	0.495757231715	0.495757231715	0.211648656965	0.211648656965
1	0.478706598832	0.478706598832	0.218213345221	0.218213345221
Distance moved by atom 1 in the positive x direction	Analytical force on atom 3 in the x-direction	Numerical force on atom 3 in the x-direction	Analytical force on atom 4 in the x-direction	Numerical force on atom 4 in the x-direction
0	-0.257069230915	-0.257069230915	-0.236635445138	-0.236635445138
0.1	-0.338090086813	-0.338090086813	-0.232026780657	-0.232026780657
0.2	-0.396303411500	-0.396303411500	-0.228303822004	-0.228303822004
0.3	-0.437962686834	-0.437962686834	-0.225355906459	-0.225355906459
0.4	-0.466695160543	-0.466695160543	-0.223087644108	-0.223087644108
0.5	-0.484697915969	-0.484697915969	-0.221418205942	-0.221418205942
0.6	-0.493505232742	-0.493505232742	-0.220279968193	-0.220279968193
0.7	-0.494398598502	-0.494398598501	-0.219616899031	-0.219616899031
0.8	-0.488581739721	-0.488581739721	-0.219382936439	-0.219382936440
0.9	-0.477227183899	-0.477227183900	-0.219540480476	-0.219540480476
1	-0.461465660331	-0.461465660331	-0.220059039661	-0.220059039661

Table 6.1 Comparison of analytical and numerical forces on atom 1 in y-direction

Distance moved by atom 1 in the positive x direction	Analytical force on atom 1 in the y-direction	Numerical force on atom 1 in the y-direction	Analytical force on atom 2 in the y-direction	Numerical force on atom 2 in the y-direction
0	-0.054107368965	-0.054107368965	0.080636084097	0.080636084097
0.1	-0.041623846943	-0.041623846942	0.075181102209	0.075181102209
0.2	-0.025029638329	-0.025029638329	0.066073809105	0.066073809105
0.3	-0.005801407510	-0.005801407510	0.054151400966	0.054151400966
0.4	0.014951936750	0.014951936750	0.040057342538	0.040057342538
0.5	0.036413427791	0.036413427791	0.024293594021	0.024293594021
0.6	0.057983435612	0.057983435612	0.007260434499	0.007260434499
0.7	0.079217767652	0.079217767652	-0.010714927052	-0.010714927052
0.8	0.099781729090	0.099781729090	-0.029358504450	-0.029358504450
0.9	0.119418518149	0.119418518149	-0.048435958660	-0.048435958660
1	0.137928567431	0.137928567431	-0.067743288466	-0.067743288465
Distance moved by atom 1 in the positive x direction	Analytical force on atom 3 in the y-direction	Numerical force on atom 3 in the y-direction	Analytical force on atom 4 in the y-direction	Numerical force on atom 4 in the y-direction
0	-0.051063618610	-0.051063618610	-0.019561987246	-0.019561987246
0.1	-0.040987459133	-0.040987459133	-0.021888614212	-0.021888614212
0.2	-0.028741038951	-0.028741038951	-0.026941023364	-0.026941023364
0.3	-0.015132293624	-0.015132293624	-0.033992787708	-0.033992787709
0.4	-0.000657430361	-0.000657430360	-0.042541731626	-0.042541731626
0.5	0.014379828210	0.014379828210	-0.052235196542	-0.052235196542
0.6	0.029786079394	0.029786079394	-0.062817203350	-0.062817203350
0.7	0.045428224009	0.045428224009	-0.074094373119	-0.074094373119
0.8	0.061206002845	0.061206002845	-0.085915200241	-0.085915200241
0.9	0.077038261115	0.077038261115	-0.098157757934	-0.098157757934
1	0.092856669310	0.092856669310	-0.110722307002	-0.110722307002

Table 6.1 Comparison of analytical and numerical forces on atom 1 in z-direction

Distance moved by atom 1 in the positive x direction	Analytical force on atom 1 in the z-direction	Numerical force on atom 1 in the z-direction	Analytical force on atom 2 in the z-direction	Numerical force on atom 2 in the z-direction
0	-0.119698158477	-0.119698158477	-0.113413198955	-0.113413198955
0.1	-0.127825866682	-0.127825866682	-0.111954133477	-0.111954133477
0.2	-0.136446272533	-0.136446272533	-0.110826785940	-0.110826785940
0.3	-0.144953537850	-0.144953537850	-0.110028566566	-0.110028566566
0.4	-0.152895817351	-0.152895817350	-0.109543211377	-0.109543211377
0.5	-0.159959002693	-0.159959002693	-0.109346965477	-0.109346965477
0.6	-0.165938142358	-0.165938142358	-0.109413322326	-0.109413322326
0.7	-0.170708506925	-0.170708506925	-0.109715992768	-0.109715992768
0.8	-0.174202060831	-0.174202060831	-0.110230426767	-0.110230426767
0.9	-0.176390634542	-0.176390634542	-0.110934382926	-0.110934382927
1	-0.177274897688	-0.177274897688	-0.111807971497	-0.111807971497
Distance moved by atom 1 in the positive x direction	Analytical force on atom 3 in the z-direction	Numerical force on atom 3 in the z-direction	Analytical force on atom 4 in the z-direction	Numerical force on atom 4 in the z-direction
0	-0.046221264055	-0.046221264055	-0.096603114301	-0.096603114301
0.1	-0.050412089960	-0.050412089960	-0.095602641243	-0.095602641243
0.2	-0.054611433443	-0.054611433442	-0.094868811573	-0.094868811573
0.3	-0.058718867904	-0.058718867904	-0.094418927064	-0.094418927064
0.4	-0.062715834715	-0.062715834715	-0.094258323386	-0.094258323386
0.5	-0.066624396184	-0.066624396184	-0.094384779920	-0.094384779920
0.6	-0.070480257711	-0.070480257711	-0.094792331587	-0.094792331587
0.7	-0.074318051068	-0.074318051068	-0.095473873734	-0.095473873734
0.8	-0.078164992095	-0.078164992095	-0.096422598917	-0.096422598916
0.9	-0.082039377610	-0.082039377610	-0.097632566556	-0.097632566556
1	-0.085951445681	-0.085951445681	-0.099098730598	-0.099098730598

Time Step (a.t.u.)	Potential Energy	Kinetic Energy	Total Energy
0.00	-21.364048196790	0.000088638515	-21.363959558276
1.00	-22.196414169609	0.832454611336	-21.363959558273
2.00	-23.990249036528	2.626289478255	-21.363959558272
3.00	-25.581711816619	4.217752258343	-21.363959558277
4.00	-26.366085822929	5.002126264649	-21.363959558281
5.00	-26.358503582788	4.994544024505	-21.363959558283
6.00	-25.825487399068	4.461527840785	-21.363959558283
7.00	-25.035898526646	3.671938968363	-21.363959558283
8.00	-24.181875485159	2.817915926876	-21.363959558283
9.00	-23.380380305858	2.016420747575	-21.363959558283
10.00	-22.695542389809	1.331582831526	-21.363959558283

Table 6.4 Conservation of energy test

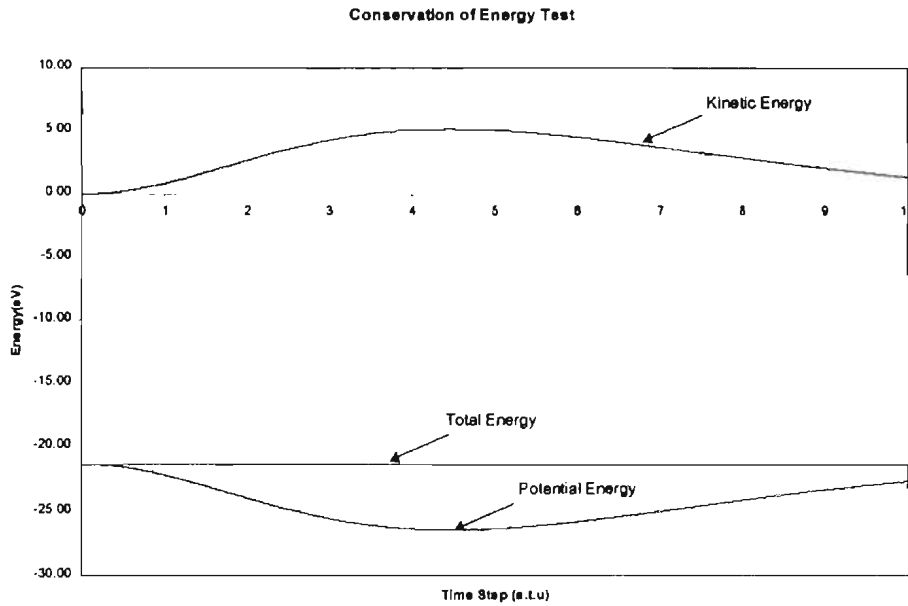


Figure 6.1 Conservation of energy test

6.3 BACK INTEGRATION

Back integration is the most sensitive of all the tests. In this test, the model, which is an isolated system, is allowed to integrate over a period of time, and then the time step is made negative, and the model is allowed to back integrate for the same period of time. The model should trace the same potential, kinetic and total energy curves in both the forward and backward integration. Also the atoms must trace the same path in both the forward and backward integration.

For this test, one lattice of Nickel is taken and allowed to integrate for a period of 100 time steps. Then the time step is made negative and the structure is allowed to back integrate for the same period of time. The potential, kinetic and total energy curves for both forward and backward integration are given in the figure 6.3. The curves overlap each other almost exactly and look as if they are the same curve. Also the position of one of the atoms in the structure is plotted against time and it traces the same path in both the directions and can be seen in the figure 6.2. These three tests validate the potential and force functions and also the integration procedure.

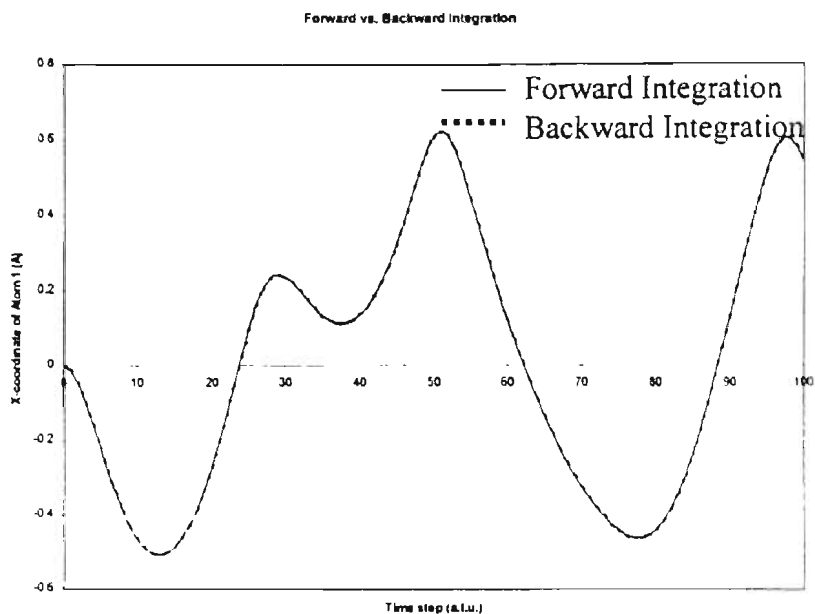


Figure 6.2 Path traced by atom 1 during forward and backward integration

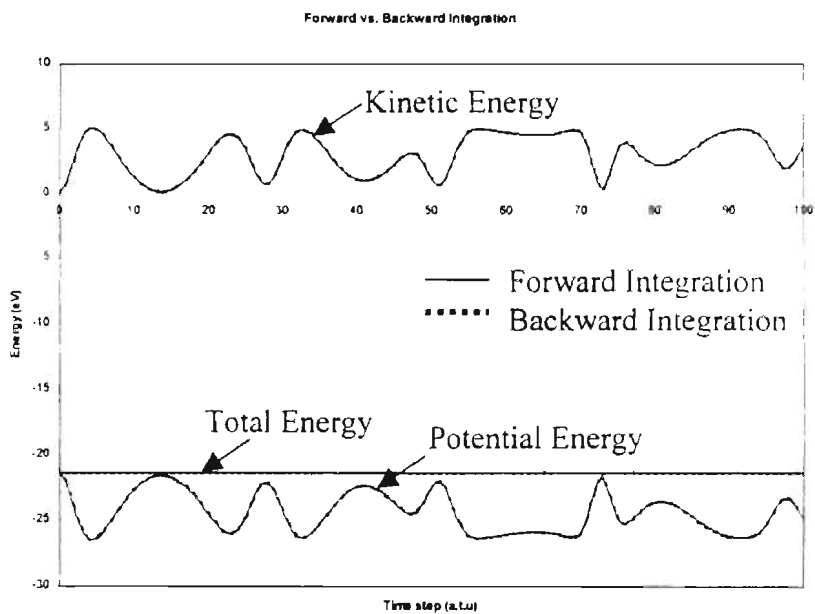


Figure 6.3 Potential, kinetic and total energies during forward and backward integration

Chapter 7

RESULTS AND DISCUSSION

7.1 INTRODUCTION

The potential model developed is good for any material with FCC, BCC, diamond structure, and HCP metals. The values are given for some of these materials in the paper by Baskes (1992). Of these, nickel, copper, and iron are selected and subjected to uniaxial tension.

7.2 TENSION TESTS

Table 7.1 shows the conditions in which the experiments are conducted.

Configuration	3 Dimensional
Potentials Used	Morse, MEAM
Work Material Dimension	4a x 4a x 6a (a = lattice constant)
Tensile Loading Condition	Uniaxial
Tension Rate	500 m/s
Bulk Temperature	293 K

The specimen has boundary (which are fixed) atoms at the top and bottom surfaces. Immediately after the boundary atoms, is a layer of peripheral atoms. The rest are moving atoms. The tension simulations are conducted at the rate of 500m/s to achieve reasonable computational time. Consequently the system temperature will increase significantly which is dissipated by means of the peripheral atoms. The motion of the atoms in the moving zone is determined solely by the forces produced by the interaction potential and the direct solution of the classical Hamiltonian equations of motion. The motion of the peripheral atoms is also calculated from the solution of Hamiltonian equations, but modified by the presence of velocity reset functions associated with each atom in the peripheral zone. In this method, the Cartesian velocity components of each peripheral lattice atoms is reset at periodic time intervals, Δt , using the following algorithm:

$$v_{\alpha i}^{new} = (1 - w)^{1/2} v_{\alpha i}^{old} + w^{1/2} V(T, \xi) \quad (8.1)$$

Where $v_{\alpha i}^{old}$ is the α -component ($\alpha=x, y, \text{ or } z$) of velocity of lattice atom i resulting from the solution of the Hamiltonian equations of motion, and $v_{\alpha i}^{new}$ is the reset α velocity component. 'w' is a parameter that controls the strength of the reset with $w=0$ corresponding to no reset and $w=1$ being a complete reset. $V(T, \xi)$ is a randomly chosen velocity from a Maxwell-Boltzmann distribution at temperature T . ξ is a random number whose distribution is uniform on the interval $[0,1]$ that controls the random selection. This procedure simulates the thermostatic effect of the bulk and guarantees that the equilibrium temperature will approach the desired value, which is 293 K in these calculations.

The animations for nickel using the MEAM and the Morse Potentials are given in figures 7.1(a)-(d) and 7.2(a)-(d). After relaxation, a light bulge in the specimen is observed, using the Morse potential as well as the MEAM potential. This is because, when the crystal relaxes, it tries to take the minimum energy position and tries to attain a spherical shape. But, since it is constrained at the top and bottom layers by boundary atoms, it bulges only on the +ve and -ve x and y-directions. The bulge is more in the case of the Morse potential than the MEAM potential. MEAM potential represents crystal surfaces better than the Morse potential. This is because MEAM potential involves calculations using electron densities and allows realistic treatment of impurities in structures that include cracks, surfaces, and alloying additions. When the tension test begins, similar behavior is observed in both the cases. The bulge decreases gradually and the specimen starts to neck. Because of the high tension rates and also because the specimen is very small, the crystal becomes amorphous almost immediately after the experiment begins. The necking continues and the diameter of the neck decreases with the increasing strain. This process continues until the specimen fails due to fracture. The stress-strain curves for the tension test of nickel using the Morse and the MEAM potentials, is given in the figure 7.3. The curves behave almost similarly until reaching the peak of the tension curves. After that, the tension curve of nickel, using the MEAM potential drops rapidly when compared to the one using the Morse potential. This can be attributed to the fact that the atoms in the tension test using the Morse potential are bonded by a pairwise potential and these bonds exist until the all the bonded pairs in the center of the specimen are out of the cutoff radius. But, in the case of the MEAM potential, the volume of the material is represented well, because the calculations are

done using the electron densities. This results in the rapid drop down in the tension curve simulating the behavior of the bulk material. Using the MEAM potential, the ultimate tensile strength is 44.46 GPa approximately at a strain of 0.31 and in the case of Morse Potential the ultimate tensile strength is 54.25 GPa approximately at a strain of 0.232.

The stress-strain curves using the MEAM potential for nickel, copper, and iron are shown in figure 7.4. The animations for the tension tests of copper, and iron using the MEAM potential, are given in figures 7.5(a)-(d) and 7.6(a)-(d). For FCC materials, nickel and copper, the simulations show reasonable behavior. Copper has a lesser ultimate tensile strength than nickel as is shown in figure 7.4. It is 25.28GPa approximately at a

	Ultimate Tensile Strength values quoted by Hertzberg (1996) (GPa)	Ultimate Tensile Strength values obtained by Komanduri et al (2000) (GPa)	Ultimate Tensile Strength values obtained by MEAM Potential (GPa)
Nickel	33.4	36.0	44.46
Copper	19.1	28.0	26.20
Iron	31.8	29.0	32.16

Table 7.2 Comparison of ultimate tensile strength values obtained by using the MEAM potential with those obtained by Komanduri et al (2000) and those quoted by Hertzberg (1996)

strain of 0.159. The strain to fracture is 0.49. The fact that the copper has lesser strength than nickel is clearly illustrated by these observations. The ultimate tensile strength of iron is 32.16 GPa approximately at a strain of 0.133 and the strain to fracture is 0.455.

Iron is found to have lesser ultimate tensile strength than Nickel but more than Copper. The ultimate tensile strength values of nickel, copper, and iron are compared with those obtained from Komanduri et al (2000) and those quoted by Hertzberg (1996) in the table 7.2. The values obtained from MEAM have the same ranking as the above

7.3 SHEAR TEST OF NICKEL

Horstemeyer and Baskes (1999) conducted a shear test of a nickel specimen of dimensions $4a \times 2a \times 2a$ at a speed of 1.0m/s and observed the shear stress vs. shear strain curves for these samples (figure 7.8). The shear stress was normalized by the elastic shear modulus of nickel (124.8 GPa). They observed a spatial size scale effect on yield stress. They used the embedded atom method as the potential model. Since embedded atom method is supported by strong physical arguments, shear of Nickel using the MEAM potential was done to compare and validate the results with those obtained by Horstemeyer et al.

A nickel sample with dimensions of $4a \times 4a \times 6a$ is taken and is subjected to shear at the speed of 500 m/s (this speed is chosen to keep the computational times reasonable), until a shear strain of 0.3. The animations are shown in figures 7.7(a)-(d). The shear stress/elastic modulus vs. the shear strain is shown in figure 7.8. It is observed that both the curves reach a peak of 0.1(approximately) for a shear strain of 0.125 (approximately). After that, the curve obtained by Horstemeyer (1999), drops down rapidly when compared to the one obtained by using the MEAM potential. This is because the shear

test of nickel using the MEAM potential is conducted at the speed of 500 m/s and this generates a lot of heat. This causes the material to become more ductile and hence increases the value of strain to fracture. The maximum shear stress/elastic modulus values are in reasonable agreement for both the curves.

The software developed is good for single crystal materials. The development and validation of the MD using MEAM was done along with Mr. David Stokes. The project consisted of five important steps, developing the code for potential function (done by me), developing the code for force function (50% by me and 50% by David), validating the potential model (50% by me, 50% by David), conducting the tension tests (done by me), and conducting the shear test (done by me). This software can be used to model other manufacturing applications like cutting, milling, and indentation by using the Morse potential as the interface potential between the tool and workpiece.



Figure 7.1a

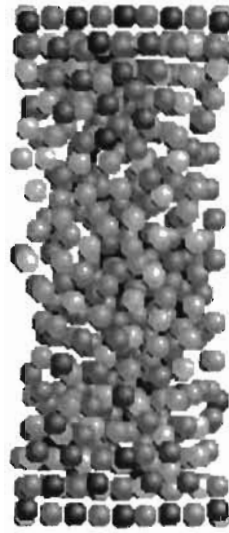


Figure 7.1b



Figure 7.1c



Figure 7.1d

Figures 7.1(a)-(d) Snapshots of animation during tension test of nickel using the MEAM potential

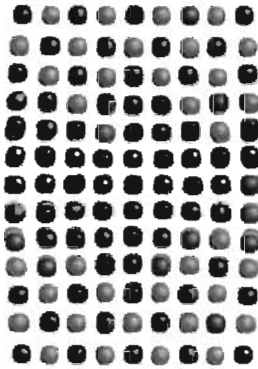


Figure 7.2 a



Figure 7.2 b

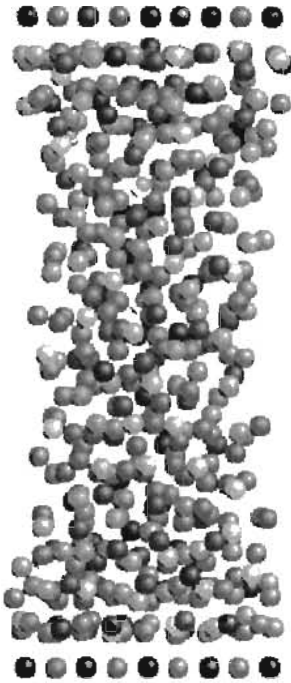


Figure 7.2 c

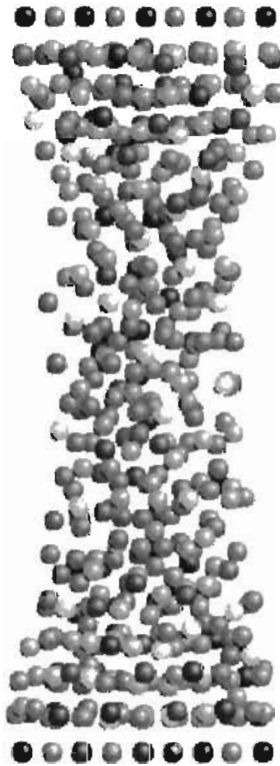


Figure 7.2 d

Figure 7.2(a)-(d) Snapshots of animation during tension test of nickel using the Morse potential

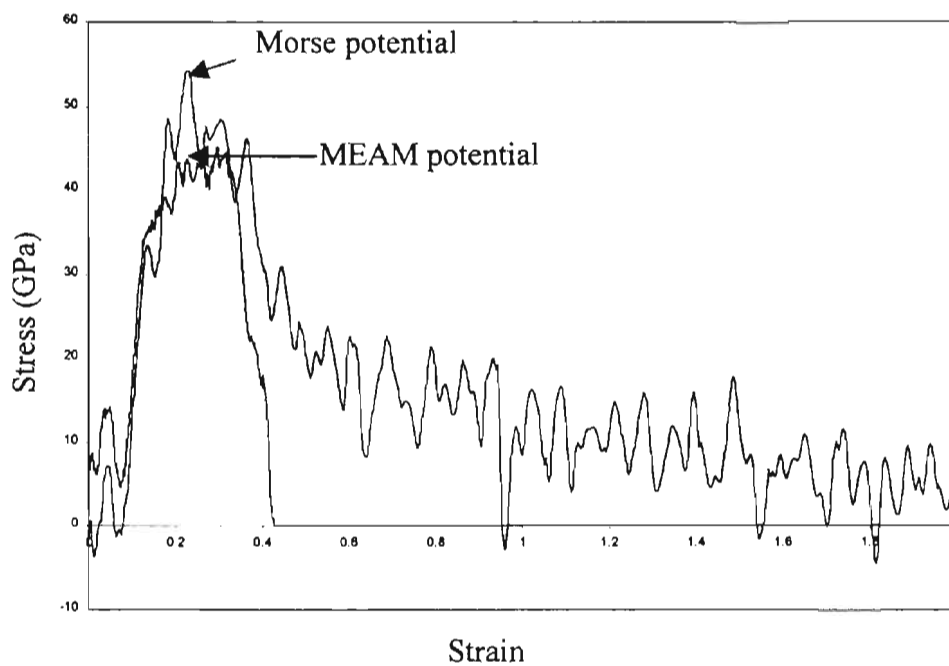


Figure 7.3 Tension test of nickel using the Morse potential and the MEAM potential

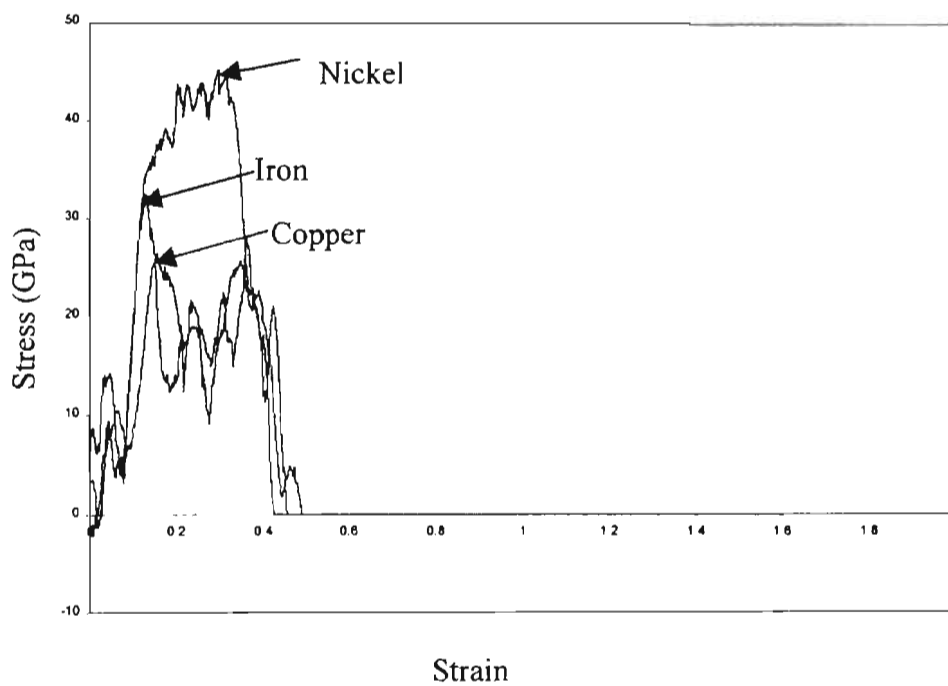


Figure 7.4 Stress vs. strain curves of nickel, copper, and iron using the MEAM potential



Figure 7.5a

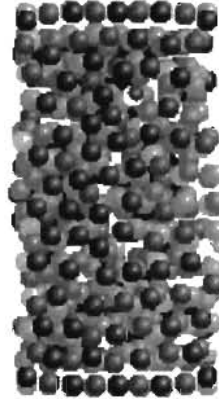


Figure 7.5b

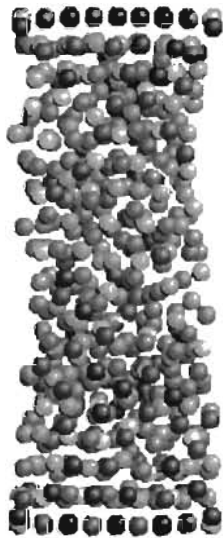


Figure 7.5c

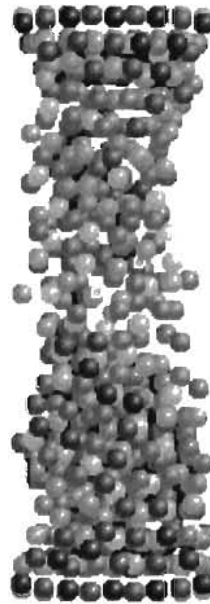


Figure 7.5d

Figures 7.5(a)-(d) Snapshots of animation during tension test of copper

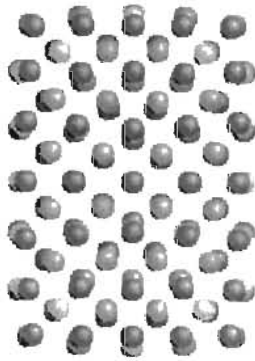


Figure 7.6a

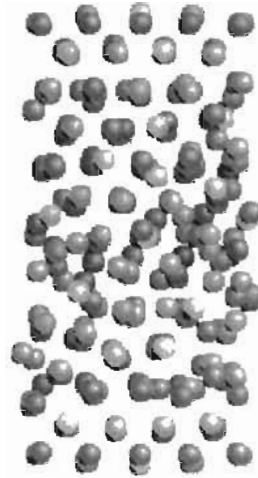


Figure 7.6b



Figure 7.6c

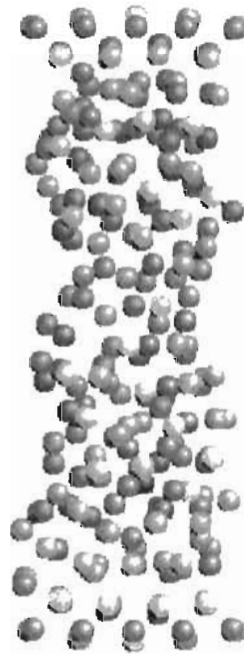


Figure 7.6d

Figures 7.6(a)-(d) Snapshots of animation during tension test of iron

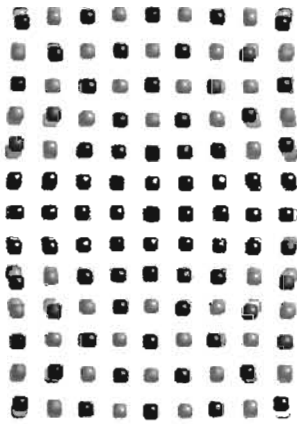


Figure 7.7a

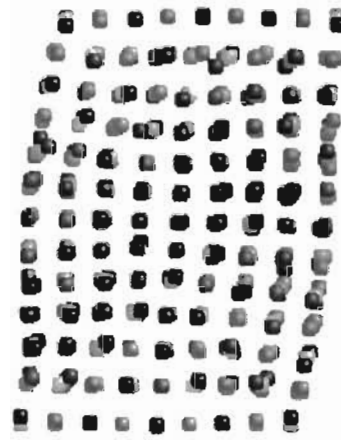


Figure 7.7b

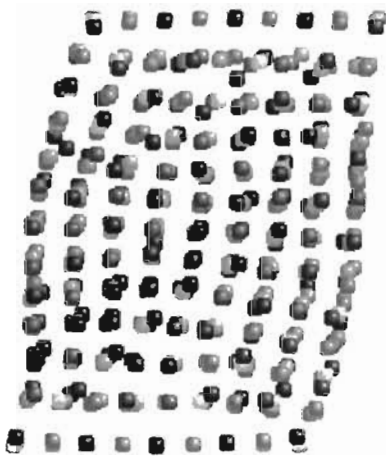


Figure 7.7c

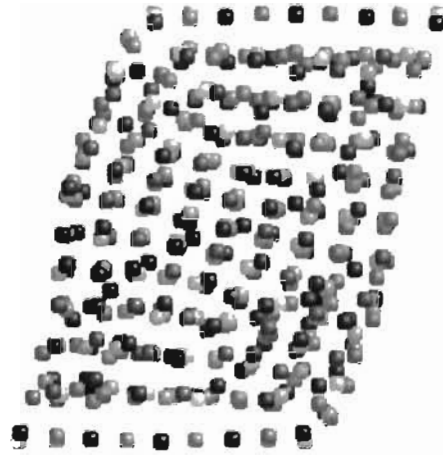


Figure 7.7d

Figures 7.7(a)-(d) Snapshots of nickel in shear

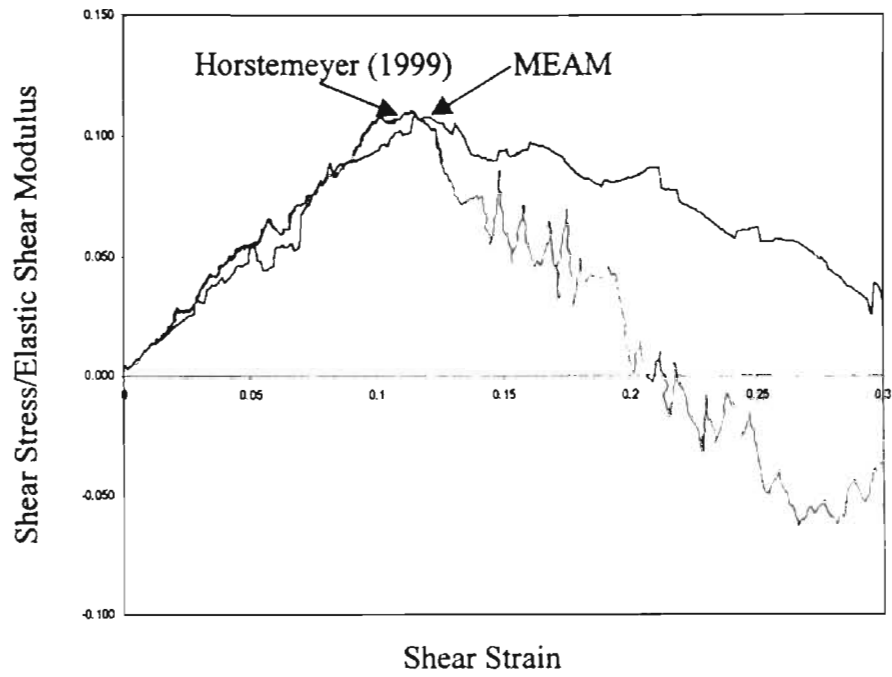


Figure 7.8 Comparison of the shear stress/elastic shear modulus vs. shear strain for nickel using the MEAM potential with that obtained by Horstemeyer (1999)

Chapter 8

CONCLUSIONS

8.1 TESTING FOR ACCURACY OF THE SOFTWARE

The “Modified Embedded Atom Method” developed by Baskes (1992) was used in the Molecular Dynamics Simulation. The following tests were conducted for determining the accuracy of the software:

1. Numerical vs. analytical forces test for the validation of the forces: A system of five-Nickel atoms was taken and one of the atoms was moved in increments of 0.1 \AA and both the analytical and numerical forces were calculated. They were in excellent agreement up to 12 significant digits
2. Conservation of energy test: Based on the fact that an isolated system should conserve energy, one lattice of Nickel was taken and allowed to integrate for a time period of 10 time steps. The total energy (sum of potential and kinetic energies) remained constant up to 12 significant digits.
3. Back Integration test: One lattice of Nickel was taken and allowed to integrate up to 100 time units and then the time step was changed to a -ve value and the system was back integrated. It traced back the same curve for kinetic, potential and total energies and the same path for the atom positions.

Based on above tests it was proved that the software developed was accurate and ready to be used.

8.2 UNIAXIAL TENSION

Uniaxial tension experiments were done on four materials: two FCC (nickel, copper) and a BCC (iron) material at 500m/s using the MEAM potential. Also, uniaxial tension of nickel, using the Morse potential, was performed and compared with the results obtained from the MEAM potential. The following observations were made:

1. The measured ultimate tensile strengths were 26.20 GPa (copper), 44.46 GPa (nickel), and 32.16 GPa (iron). These values have the same ranking as the theoretical values of defect free whiskers given in Hertzberg (1998) and also as those obtained by Komanduri et al (2000).
2. Copper has the least strength (26.20 GPa) while nickel has the highest strength (44.46 GPa) among the three materials. In bulk also, copper has the least strength of the three materials and nickel has the highest.
3. The strain to fracture at room temperature for Cu, Ni, and Fe, 0.493, 0.43, and 0.461 respectively. Copper exhibited the maximum ductility undergoing a maximum strain of 0.493 before failure.

By the above observations it is clear that the MEAM potentials represent both the FCC and BCC materials fairly well and can be used to perform tensile testing of these materials.

8.3 SHEAR TEST OF NICKEL

Shear test of Nickel was conducted at a speed of 500m/s and the shear stress, which was normalized by dividing it with the elastic shear modulus of Nickel (124.8 GPa) vs. shear strain was plotted. The curve reached a maximum of ~ 0.1 at a shear strain of ~ 0.125 . The value of maximum shear stress/ elastic modulus was in reasonable agreement with that obtained by Baskes and Horstemeyer (1999). After reaching the peak, the curve obtained by MEAM dropped less rapidly than that obtained by Horstemeyer. The difference is attributed to the fact that the shear test conducted by using the MEAM potential was conducted at a high speed, and this increased the temperature of the specimen. This lead to higher ductility and increased value of strain to fracture.

8.4 FUTURE WORK

1. The existence of stray atoms might be because of the small specimen sizes. Due to time constraint on this project, the experiments were conducted with smaller sizes. Experiments must be conducted using large sizes to find out the size-scale effects on the ultimate tensile strength and strain to fracture.
2. The model developed above is good for single crystal materials. It can be used to define the potential between like atoms. An alternate potential model like the Morse potential can be used to define the potential between unlike atoms. Then this model can be extended to other manufacturing applications like cutting, milling, and indentation, where the Morse potential can be used to define the interactions between tool and workpiece (unlike atoms).

3. Crystals with defects and cracks can be modeled using the MEAM potential. This can be done by introducing a defect by removing few atoms randomly from the workpiece to simulate a defect, or by removing few atoms from the workpiece in the shape of the crack to be studied to simulate a crack. Uniaxial tension and shear experiments should then be conducted on materials to study their effects on the tensile properties.

REFERENCES

- Adams, J.B., Foiles, S.M., "*Development of an Embedded Atom Potential for a BCC Metal: Vanadium*," Physical Review B, 41/6, pp.3316-3327, 1990.
- Allen, M., and Tildesley, D., "*Computer Simulation of Liquids*," Oxford University Press, Oxford, U.K, 1991.
- Alder, B.J., Wainwright, T.E., "*Studies in Molecular Dynamics. I. General Method*," The Journal of Chemical Physics, 31/2, pp.459-466, 1959.
- Baskes, M.I., Daw, M.S., "*Semi-empirical, Quantum Mechanical Calculation of Hydrogen Embrittlement in Metals*," Physical Review Letters, 50/17, pp.1285, 1983.
- Baskes, M.I., Daw, M.S., "*Embedded Atom Method: Derivation and Application to Impurities, Surfaces, and other Defects in Metals*," Physical Review B, 29/12, pp.6443-6453, 1984.
- Baskes, M.I., Foiles, S.M., Daw, M.S., "*Embedded Atom Method functions for Cu, Ag, Au, Ni, Pd, Pt, and their alloys*," Physical Review B, 33/12, pp.7983-7991, 1986.
- Baskes, M.I., "*Application of the Embedded-Atom Method to Covalent Materials: A Semi-empirical Potential for Silicon*," Physical Review Letters, 59, pp.2666, 1987.
- Baskes, M.I., Foiles, M.F., Daw, M.S., "*Atomistic Studies of Interfacial Structure and Properties*," Materials Research Soc. Symp. Proc., 122, pp.343-353, 1988.
- Baskes, M.I., Nelson, J.S., Wright, A.F., "*Semi-empirical Modified Embedded Atom Potentials for Silicon and Germanium*," Physical Review B, 40/9, pp.6085-6100, 1989.
- Baskes, M.I., "*Modified Embedded Atom Potentials for Cubic Materials and Impurities*," Physical Review B, 46/5, pp.2727, 1992.

- Baskes, M.I., "*MEAM for HCP Metals*," Modeling Simulation Mater. Sci. Eng., 2, pp.147, 1994.
- Baskes, M.I., "*Determination of Modified Embedded Atom Method Parameters for Nickel*," Materials Chemistry and Physics, 50, pp.152-158, 1997.
- Belak, J., Boercker, D.B., Stowers, I.F., "*Simulation of Nanometer-Scale Deformation of Metallic and Ceramic Surfaces*," MRS Bulletin, pp.55-60, 1993.
- Chandrasekaran, N., "*Length Restricted Molecular Dynamics Simulation of Nanometric Cutting*," Thesis, Oklahoma State University, 1997.
- Daw, M.I., "*Model of Metallic Cohesion: The Embedded Atom Method*," Physical Review B, 39/11, pp. 7441-7451, 1989.
- Eyring, H., Walter, J., Kimball, G.E., "*Quantum Chemistry*," John Wiley & Sons, Inc., 1944.
 - Haile, J., "*Molecular Dynamics Simulation Elementary Methods*," John Wiley & Sons, Inc, 1992.
- Heino, P., Hakkinen, H., Kaski, K., "*Molecular Dynamics Study of Mechanical Properties of Copper*," Europhysics Letters, 41/3, pp.273-278, 1998.
- Hertzberg, R.W., "*Deformation and Fracture Mechanics of Engineering Materials*," 4th Edition, John Wiley & Sons, NY, 1996.
- Horstemeyer, M.F., Baskes, M.I., "*Atomistic finite deformation simulations: A discussion on length scale effects in relation to mechanical stresses*," Journal of Engineering Materials and Technology, 121/2, pp.114-119, 1999.

Kitamura, T., Yashiro, K., Ohtani, R., "***Atomistic Simulation on Deformation and Fracture of Nano-Single Crystal of Nickel in Tension***," JSME Int. A, 40/4, pp.430-435, 1997.

Komanduri, R., Chandrasekaran, N., Raff, L.M., "***Molecular Dynamics Simulation of Uniaxial Tension***," submitted for publication.

Lynden-Bell, R.M., "***Computer Simulation of Fracture at Atomistic Level***," J. Phy. Condens. Matter, 4, pp.1704-1705, 1994.

Lynden-Bell, R.M., "***A Simulation Study of Induced Disorder, Failure and Fracture of Perfect Metal Crystals under Uniaxial Tension***," J. Phy. Condens. Matter, 7, pp.4603-4624,1995.

Raff, L.M., and Thompson, D.A., "***The Classical Trajectory Approach to Reactive Scattering***," Chapter 1, Volume 3 in Theory of Chemical Reaction Dynamics, Ed. Michael Baer, CRC Press, 2-121, 1986.

• Rappaport, D.C., "***The art of Molecular Dynamics Simulation***," Cambridge University Press, 1995.

Rentsch, R., Inasaki, I., "***Indentation Simulation on Brittle Materials by Molecular Dynamics***," Annals of CIRP, 44/1, pp.295, 1995.

Sato, K., Yoshioka, T., Ando, T., Shikida, M., Kawabata, T., "***Tensile Testing of Silicon Film Having Different Crystallographic Orientations Carried out on a Silicon Chip***," Sensors and Actuators, A 70, pp.148-152, 1998.

Stewart, R., "***Investigation on Molecular Dynamics Simulation of Nanometric Cutting***," Thesis, Oklahoma State University, 1998.

Stott, M.J., Zaremba, E., "*Quasiatoms: An Approach to Atoms in Nonuniform electronic systems*," Physical Review B, 22/4, pp.1564-1583, 1982.

Voter, A.F., Chen, S.P., Mater. Res. Soc. Symp. Proc., 82, pp.175, 1987.

Yi, T., Li, L., Kim, C.J., "*Microscale Material Testing of Single Crystal Silicon: Process Effects on Surface Morphology and Tensile Strength*," Sensors and Actuators, 83, pp.172-178, 2000.

VITA

Kalyan K. Mavuleti

Candidate for the Degree of

Master of Science

Thesis: MOLECULAR DYNAMICS SIMULATION USING THE MODIFIED
EMBEDDED ATOM METHOD

Major Field: Mechanical Engineering

Biographical:

Personal Data: Born in Gudivada, India, on January 3, 1976, the son of Ganga Raju Mavuleti and V.V. Subramanyeswari Mavuleti

Education: Received Bachelor of Technology degree in Mechanical Engineering from Jawaharlal Nehru Technological University, Kakinada in June 1998. Completed the requirements for the Master of Science degree with a major in Mechanical Engineering at Oklahoma State University in Oct, 2000.

Experience: Research Assistant in Oklahoma State University from August '98-December 2000.